Dual production of polyhydroxyalkanoates and antibacterial/antiviral gold nanoparticles

frontiers | Frontiers in Nanotechnology

TYPE Original Research
PUBLISHED 07 September 2023
DOI 10.3389/fnano.2023.1243056

OPEN ACCESS

EDITED BY
Lukas Gritsch,
Technogym S.p.A., Italy

REVIEWED BY
Wei Shao,
Westlake University, China
Shailesh S. Sawant,
Rural Development Administration, Republic of Korea
Justyna Mozejko-Ciesielska,
University of Warmia and Mazury in Olsztyn, Poland

*CORRESPONDENCE
Pooja Basnett,
p.basnett@westminster.ac.uk
Adele McCormick,
a.mccormick@westminster.ac.uk

†These authors share first authorship

‡These authors share last authorship

RECEIVED 20 June 2023
ACCEPTED 07 August 2023
PUBLISHED 07 September 2023

CITATION
Paxinou A, Marcello E, Vecchiato V, Erman L, Wright E, Noble B, McCormick A and Basnett P (2023), Dual production of polyhydroxyalkanoates and antibacterial/antiviral gold nanoparticles. *Front. Nanotechnol.* 5:1243056. doi: 10.3389/fnano.2023.1243056

Dual production of polyhydroxyalkanoates and antibacterial/antiviral gold nanoparticles

Alexandra Paxinou[1,2†], Elena Marcello[1,3†], Vittoria Vecchiato[1], Lara Erman[1], Edward Wright[4], Brendon Noble[1], Adele McCormick[1,5*‡] and Pooja Basnett[1*‡]

[1]Sustainable Biotechnology Group, School of Life Sciences, College of Liberal Arts and Sciences, University of Westminster, London, United Kingdom, [2]Foundation of Research and Technology Hellas, Institute of Chemical Engineering and High Temperature Chemical Processes (FORTH/ICE-HT), Patras, Greece, [3]Department of Mechanical and Aerospace Engineering, Politecnico di Torino, Turin, Italy, [4]Viral Pseudoptype Unit, School of Life Sciences, University of Sussex, Falmer, United Kingdom, [5]Genomics and Infection Diseases Research Group, School of Life Sciences, College of Liberal Arts and Sciences, University of Westminster, London, United Kingdom

Gold nanoparticles (AuNPs) have been explored for their use in medicine. Here, we report a sustainable, and cost-effective method to produce AuNPs using a bacterial strain such as *Pseudomonas mendocina* CH50 which is also known to be a polyhydroxyalkanoate (PHA) producer. A cell-free bacterial supernatant, which is typically discarded after PHA extraction, was used to produce spherical AuNPs of 3.5 ± 1.5 nm in size as determined by Transmission Electron Microscopy (TEM) analysis. The AuNPs/PHA composite coating demonstrated antibacterial activity against *Staphylococcus aureus* 6538P, and antiviral activity, with a 75% reduction in viral infectivity against SARS-CoV-2 pseudotype virus.

KEYWORDS

polyhydroxyalkanoates, gold nanoparticles, dual production, antimicrobial coatings, antibacterial, antiviral, SARS-CoV-2

1 Introduction

Microbial contamination poses a social and economic challenge worldwide. Within the expansive family of microbes, bacteria and viruses are considered to be the most threatening to human health. Microbial infections are associated with the growing increase of antimicrobial resistance (AMR) which is listed by the World Health Organization (WHO) as one of the top 10 global public health threats (Okkeh et al., 2021). The last decade has seen a steady rise in multi-drug resistance species, of which, the numbers of the two main pathogens *Escherichia coli* (MDR) and *Staphylococcus aureus* (MRSA) are projected to increase by 2050 (Barber and Sutherland, 2017; Murray, 2022). The problem is exacerbated by the misuse of antibiotics along with the drastic decrease in the number of new drugs being discovered (Riberio da Cuncha et al., 2019). In tandem, the continuous evolution of new viruses presents an emerging global challenge. The severe acute respiratory syndrome coronavirus 2 (SARS-CoV-2) has had a global impact and is still posing a significant humanitarian challenge with a count of approximately 6,955,497 (World Health organization, 2023) deaths sore far. COVID-19 outbreak has led to a significant increase in inappropriate antibiotic usage, favoring and worsening AMR nosocomial

dissemination (World Health Organization, 2022). Therefore, it is vital to foster innovation in the optimisation of the efficacy of existing drugs and other approaches to control viruses in addition to seeking new antiviral treatments, whereby vaccine efficacy is compromised by emerging variants (Dickey et al., 2017).

One such promising area is medical nanotechnology, which has proved to be effective in treating complex health problems (Okkeh et al., 2021). Notably, amongst the inorganic nanomaterials, gold nanoparticles (AuNPs) have attracted great attention as antiviral/antimicrobial materials. Previous studies have validated their suitability as biosensors, detection and imaging agent and as drug and gene delivery carriers (Wu and Ng, 2017). This is due to their biocompatibility, suitability for surface functionalisation, high surface area to volume ratio, efficient contact with microorganisms and faster ion release kinetics compared to the equivalent bulk materials and optical features (Reidy et al., 2013; Palza, 2015; Anik et al., 2022). The mechanism of action of metal NPs is still contentious. Many studies suggest that the antibacterial activity is based on the release of ions, which then can lead to bacterial death by different pathways, including ROS generation, thiol depletion or protein denaturation (Palza, 2015; Kędziora et al., 2018). Alternatively, it has been hypothesised that NPs interact with the cell membrane causing its disintegration leading to increased permeability (Slavin et al., 2017).

Standard method for the synthesis of metal NPs (MNPs) involves the use of chemical (i.e., chemical reduction using a reducing agent), physical (e.g., irradiation, photochemical treatment) or mechanical processes (e.g., ultra-sonication). However, they have limitations, such as low yield, high cost, use of toxic chemicals, and high energy requirements (Chen et al., 2007; Khaydarov et al., 2009; Liu et al., 2017; Naikoo et al., 2021). Alternatively, more sustainable approaches are currently being explored to reduce the environmental impact of MNPs production methods, while improving their efficacy as pharmaceuticals and antiviral/antimicrobial nanomaterials (Lahiri et al., 2021). MNPs can be synthesised via environmentally friendly methods using biological sources such as bacteria, fungi, and plant extracts (Silambarasan and Abraham, 2012; Yugandhar et al., 2018). The route for microbial biosynthesis of MNPs can be either intracellular or extracellular (Sharon, 2012; Nichols et al., 2009; Silambarasan and Abraham, 2012; Mohd Yusof et al., 2019). Enzymes, proteins and other compounds secreted by the bacterial cells are known to be responsible for the reduction of heavy metals into MNPs; nevertheless, the exact mechanism of MNPs production by bacterial cells is yet to be elucidated (Mohd Yusof et al., 2019).

Research on AuNPs, although currently limited, is promising. More research is needed to fully explore their potential for targeted drug delivery and antiviral/antibacterial applications. One potential nosocomial application is to incorporate MNPs within the polymer matrix to develop antibacterial and antiviral coatings applicable in healthcare settings. Bio-based polymers, specifically Polyhydroxyalkanoates (PHAs), have become well known in the development of antiviral/antimicrobial coatings and films. PHAs are biodegradable, nontoxic and biocompatible materials, that have been extensively explored for their biomedical uses. Depending on the enclosed/conjugated medicinal agent, they have been investigated for anti-inflammatory, antifungal, antimicrobial, and antiviral, purposes (Ladhari et al., 2023). PHAs are a family of thermoplastic polymers produced intracellularly by a variety of bacterial species. Additionally, PHAs can be produced by bacteria using renewable, waste streams such as waste frying oil (WFO) making them a sustainable alternative over petroleum derived polymers. Around 29 million tonnes of WFO are generated annually as a byproduct of food processing industries (Maddikeri et al., 2012). The current end-of-life management of WFO is suboptimal and raises important environmental concerns due to its mishandling. Previous studies have reported the use of WFO as a carbon substrate to produce PHAs allowing the valorisation of waste into a value-added product, thereby, decreasing environmental impact of WFO (Vidal-Mas et al., 2001; Fernández et al., 2005; Haba et al., 2007; Song et al., 2008; Verlinden et al., 2011; Kourmentza et al., 2018).

In this study, we investigated the dual sustainable production of PHAs and gold NPs (AuNPs) by *Pseudomonas mendocina* CH50 using WFO as the sole carbon source. We developed a biopolymer-based coating intended for their use in the hospital environment, by incorporating AuNPs within the PHA matrix. Antibacterial and antiviral properties of the developed biobased coating were tested using *S. aureus* and *E. coli*, and SARS-CoV-2 spike pseudotype virus respectively. The schematic of the study is presented in Figure 1.

2 Materials and methods

2.1 Materials

All the reagents, chemicals and consumables were procured from Sigma-Aldrich Company Ltd., (United Kingdom), Thermo Fisher Scientific (United Kingdom), National Institute of Biological standards and Control (NIBSC), STARLAB and VWR International (United Kingdom). Waste frying oil was obtained from the University of Westminster, Cavendish campus cafe.

2.2 Revival of the bacterial strains

A loopful of *P. mendocina* CH50 stock procured from the National Collection of Industrial and Marine Bacteria (NCIMB 10542) was streaked onto a sterile nutrient agar plate and cultured at 30°C for 16 h. A single colony of *P. mendocina* CH50 was added to 100 mL of sterile nutrient broth and cultured at 30°C for 16 h at 200 rpm. Stock cultures were prepared using sterile glycerol solution and the vials were stored at −80°C. For antibacterial studies, *Staphylococcus aureus* 6538P and *Escherichia coli* 8739 were purchased from the American Type Culture Collection (ATCC). They were revived by culturing in sterile nutrient broth at 37°C for 16 h at 200 rpm. Stock cultures were made using 20% sterile glycerol solution and the vials were stored at −20°C, for routine usage or at −80°C for extended storage.

2.3 Biosynthesis of PHAs

PHA was produced by *P. mendocina* CH50 using 20 g/L waste frying oil as the sole carbon source. The production was carried out in a 14 L Applikon ez-Control bioreactor, (Getinge Applikon). Batch fermentation was carried out in two stages as described by Lukasiewicz et al. (Lukasiewicz et al., 2018). The culture was grown for 48 h, at 30°C, and at 200 rpm with an air flow rate of 1 vvm. The temporal profile of the PHA production by *P. mendocina*

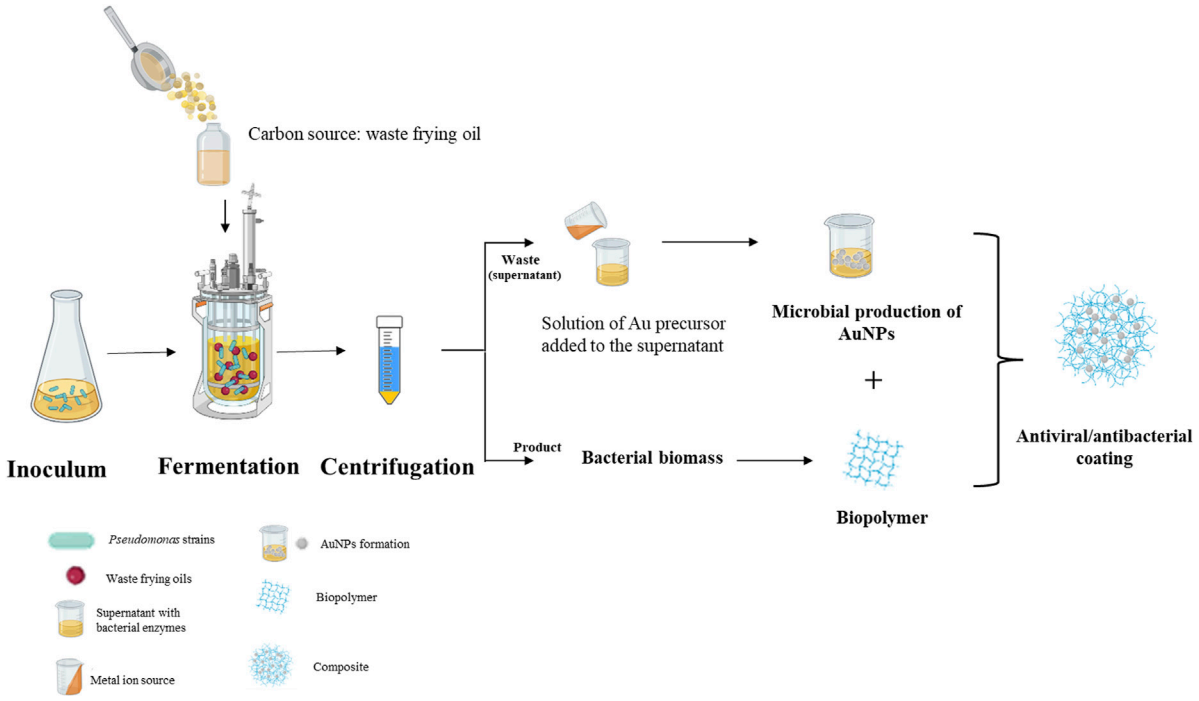

FIGURE 1
Overview of the process for the fabrication of the antiviral/antibacterial coating.

CH50 was obtained by monitoring optical density (OD_{450}), biomass, pH, nitrogen, and dissolved oxygen tension (%DOT) at regular intervals during the fermentation process. The OD was monitored at 450 nm throughout the fermentation process by sampling the culture at interval time point of 3 h, using SB038 (Cadex, Richmond, Canada) spectrophotometer. Phenol-hypochlorite method (Rai et al., 2011) was used in order to estimate nitrogen concentration in the ammonia form. An amount of 250 µL of the respective sample was incubated with 100 µL of nitroprusside reagent and 150 µL of alkaline reagent protected from light for 45 min. The absorbance was read at 635 nm and ammonium sulphate was used as the standard. Nitrogen concentration was calculated from the calibration curve prepared using ammonium sulphate standard. After the completion of the fermentation process, the cells were centrifuged at 4600 rpm for 20 min. Biomass was collected, washed with distilled water to remove impurities, and lyophilised using a freeze dryer (Labconco, 6L -84 Series) for 48 h prior to extraction. Supernatant (cell-free extract) was collected and stored at 4°C for further use. PHA was extracted from the dried biomass using soxhlet apparatus as described by Basnett et al., (Basnett et al., 2017).

2.4 Biosynthesis of AuNPs

Supernatant (cell-free extract) was used for the synthesis of gold nanoparticles. 1 mL of hydrogen tetrachloroaurate ($HAuCl_4$) was added to an aliquot of 25 mL of cell free supernatant. The reaction mixture was incubated at 37°C for 24 h. The reduction of Au^+ ions was visually detected by the change from its initial yellow to reddish colour. Cell free supernatant without $HAuCl_4$ was used as the negative control.

2.5 Characterisation of the PHAs

2.5.1 Attenuated total reflectance fourier transform infrared (ATR-FTIR) spectroscopy

Fourier transform infra-red (FT-IR) spectroscopy was used to analyse the functional groups present in the polymer. The analyses were performed in a spectral range of 4000 to 400 cm^{-1} with a resolution of 4 cm^{-1} using PerkinElmer FT-IR spectrometer Spectrum Two (PerkinElmer Inc., United States).

2.5.2 Gas chromatography mass spectrometry (GC-MS)

The monomer units of the polymer were identified using a Varian GS/MS system consisting of Chrompack CP-3800 gas chromatograph and Saturn 200 MS/MS block, using reference standards of methyl esters of 3-hydroxyalkanaotes: 3-hydroxybutyrate (3HB), 3-hydroxyhexanoate (3HHx), 3-hydroxyoctanoate (3HO), 3-hydroxydecanoate (3HD), 3-hydroxydodecanoate (3HDD). 1 mL/min of the methanolysed sample was injected at 225°C using helium as the carrier gas. The column temperature was increased from 40 to 240°C at 18°C/min and held at the final temperature for 10 min.

2.5.3 Differential scanning calorimetry (DSC)

The thermal properties of the polymer were studied using differential scanning calorimetry 214 Polyma (Netzsch, Germany)

equipped with Intracooler IC70 cooling system. 5 mg of sample was heated, cooled, and then heated again between −70°C and 170° at a heating rate of 10°C min^{-1}. The thermograms were analysed using *Proteus* 7.0 software. The obtained thermogram provided the values of the melting temperature (T_m) and the glass transition temperature (T_g).

2.5.5 Surface wettability -water contact angle

The wettability of the PHA films were studied using Theta Lite optical tensiometer (Biololin Scientific, Manchester, United Kingdom). 200 µL of deionized water was dropped onto the surface of the film samples using a gas-tight micro-syringe. The contact angle of the droplet on the specimen's surface was recorded with 10 images, captured with a frame interval of one second. All experiments were carried out in triplicates and the mean value was calculated.

2.6 Characterisation of the bio-fabricated AuNPs

2.6.1 UV–vis spectroscopy analysis

The visual change from the initial yellow to reddish colour indicates the occurrence of the redox reaction transforming Au^{3+} ions from the excited state to Au° ground state. Additionally, UV–visible spectrophotometer measures the surface plasmon resonance (SPR) at 530 nm revealing the excitation spectra of AuNPs, confirming the reduction of $HAuCl_4$ to AuNPs.

2.6.2 Analysis by transmission electron microscopy (TEM)

The size and morphology of bio-synthesised AuNPs, were investigated using high resolution transmission electron microscope Jeol/JEM 2100 0.13 nm resolution Japan, operated at 200 kV. A drop of the sonicated aqueous suspension of AuNPs was dropped on carbon coated copper HR-TEM grid. The copper grid was set aside for drying at room temperature.

2.6.3 Dynamic light scattering (DLS)

Dynamic Light Scattering (DLS) experiments were performed using a Horiba SZ-100 Dynamic Light Scattering Particle-Analyzer and the data were analysed using the Horiba software (version 2.4).

2.6.4 Antibacterial activity of the bio-synthesised AuNPs

The antibacterial activity of AuNPs were evaluated using ISO 20776 against Gram-positive and Gram-negative bacterial strains, *S. aureus* 6538P and *E. coli* 873, respectively. A range of concentrations of the AuNPs (5–100 mg/mL) suspended in Mueller Hinton broth was mixed with the microbial suspension adjusted to achieve a final concentration of 5×10^5 CFU/mL. They were incubated at 37°C for 24 h at 100 rpm in 96 multi-well plates (final volume 100 µL). After the incubation time, the OD_{600} of the wells was measured to determine the minimum inhibitory concentration (MIC) value of the AuNPs for each bacterial strain. The entire volume (100 µL) of the well containing AuNPs identified as the MIC and of the wells with a concentration higher than the MIC were spread evenly onto agar plates. The plates were incubated at 37°C for 24 h. After the incubation time, the colony forming units (CFU) were counted and compared to the CFU/mL of the initial inoculum. The Minimum Bactericidal Concentration (MBC) value was ascertained as the minimal concentration of compound that induced 99.9% killing of the bacteria.

2.6.5 Production of SARS-CoV-2 spike pseudotype virus

SARS-CoV-2 spike pseudotyped HIV-1 luciferase particles were produced by transfection of HEK293T/17 cells (ATCC, Cat no: CRL-11268) with 1ug pCAGGS-SARS-CoV-2 Spike expressing plasmid (CFAR, cat no: 100976; sequence of spike from Wuhan-Hu-1 isolate Genbank MN908947.3), 1ug p8.91 HIV-1 *gag-pol* and *rev* 2nd generation lentiviral packaging plasmid and 1.5 µg pCSFLW (lentiviral vector expressing firefly luciferase reporter (Carnell et al., 2015). Plasmids were mixed with Opitmem (GIBCO, Thermofisher Cat no: 51985034) and 1 mg/mL polyethylenimine (PEI, Sigma Cat No: 408727-100 ML) at a 1:5 ratio (DNA:PEI). Following transfection in 10 cm plastic Petri dishes (Nunc™, ThermoFisher cat no:1503500), viral supernatant was collected at 48 h and 72 h after transfection, filtered through a 0.4 µm filter (STARLAB, cat no: E4780-1453) and stored at −80°C. The 50% tissue culture infectious dose ($TCID_{50}$) of SARS-CoV-2 pseudotype virus was determined using the Bright-Glo luciferase assay system (Promega cat no: E2650), including a luminometer (Glomax Multi Detection System Luminometer, Promega cat no: E7041).

2.6.6 Antiviral screening of the bio-synthesised AuNPs

The antiviral activity against SARS-CoV-2 lentiviral pseudotype virus of the AuNPs were investigated following an adapted ISO protocol. AuNPs at a concentration of 1 µg/mL were prepared in DMEM culture media and inoculated with 50 µL ($TCID_{50}$ 1.16×10^6/mL) of SARS-CoV-2 pseudotype virus at room temperature for 24 h in a 96 multi-well plate. The following day, 100 µL of each sample was transferred to a 96-well white plate (Thermo Fisher cat no: 136101) and 2-fold dilutions were performed across the plate in 100 µL DMEM containing 10% FBS and 1% penicillin/streptomycin, and the necessary controls were included in parallel (compound only, cell control and virus control). Following this, 100 µL of 2×10^4/well HEK293T + ACE2+TMPRSS2 (human embryonic kidney cells expressing angiotensin-converting enzyme 2 and transmembrane protease serine 2, NIBSC cat no:101008) were added to each well of the 96 well white plate and incubated for 48 h at 37°C (5%CO_2). Then, a 50:50 mix of Bright-Glo (Promega, United Kingdom) and serum-free DMEM media (Sigma Cat No:D6429) was added to each well and the reporter activity assessed using Glomax Multi Detection Luminometer (Promega, United Kingdom) and the % reduction in viral infectivity was determined using formula (U−T)/U*100. Where U is the amount of virus in RLU for the virus control sample, and T is the amount of virus in RLU for virus treated with AuNPs.

2.6.7 *In vitro* cytocompatibility of the bio-synthesised AuNPs

The cytocompatibility of the AuNPs was investigated following the ISO 10993-5 guidelines, measuring the cell viability using

Alamar Blue® Cell Viability Assay. 20000 HEK-293T cells per well were seeded on to a 96 well tissue culture plate and incubated at 5% CO_2, at 37°C, for 24 h. Following this, the cell media was removed from each well and the cells were exposed to increasing concentrations of AuNPs (0.07–20 mg/mL in DMEM high glucose, 100 µL final volume), and incubated for 24 h. Cells cultured in cell culture media without AuNPs were used as a negative control. After 24 h, the supernatant was removed, and the cells were incubated with 100 µL of 10% Alamar Blue solution for 4 h. After the incubation period, the absorbance was measured at 570 and 600 nm and cell viability were calculated according to manufacture instructions.

2.7 Fabrication of coatings based on PHA and AuNPs

To develop biobased coatings, 2% w/v PHA solution in chloroform containing 10% w/w of AuNPs were stirred for 24 h and sonicated for 10 min 2% w/v PHA solution without AuNPs was used as the negative control. 20 µL of the polymer solution were applied over the Polyethylene terephthalate (PET) discs of 6 mm in diameter and allowed to dry for 72 h at room temperature (Dinjaski et al., 2014).

2.7.1 Scanning electron microscopy of composite coatings (SEM)

The surface morphology of the composite coatings produced as described above was investigated using a beam of 5 keV at 10 cm working distance (JEOL 6700 FE SEM).

2.7.2 Antibacterial test for direct contact Test—ISO 22196

The antibacterial properties of the composite films were evaluated following the ISO 22196 against *S. aureus* 6538P. Coating samples were sterilised by UV light for 15 min, placed onto agar plates, inoculated with 10 µL of a bacterial culture adjusted to a concentration of 3–5 × 10^5 CFU/mL and incubated in static conditions at 37°C for 24 h. After the incubation time, the bacteria were recovered from the sample using PBS solution and the number of viable cells were determined through the colony-forming unit method using the drop plate technique (Herigstad et al., 2001). PHA solution without AuNPs were used as the negative control. The antibacterial activity was expressed as the % reduction of the number of cells, which was calculated using the formula:

$$\%\ \text{bacterial cell reduction} = (U - T)/U^*100$$

where U is the number of viable bacteria recovered from the control samples, and T is the number of viable bacteria from samples containing AuNPs.

2.7.3 Antiviral test for the coatings

The antiviral properties of the composite films were evaluated following ISO 18184 against SARS-CoV-2 pseudotype virus. Sample coatings 6 mm in diameter were sterilized by UV light for 15 min, placed in 96 multiwell plate and inoculated with 25 µL of ($TCID_{50}$ 1.16 × 10^6/mL) of SARS-CoV-2 pseudotype virus at room temperature for 24 h. The following day, virus was recovered from the coatings with DMEM containing 10% FBS and 1% penicillin/streptomycin, and transferred to a 96-well white plate, and samples diluted to reach non-toxic levels prior to 48 h infection of 2 × 10^4/well HEK293T cells that express ACE-2 and TMPRSS2. Again, the necessary controls were included in parallel (media from coating only, cell control and virus control). Luminescence was measured using Bright-Glo Luciferase assay system (Promega, United Kingdom). The % reduction in viral infectivity was determined using formula (U−T)/U*100. Where U is the amount of virus in RLU in the absence of coatings and T is the amount of virus in RLU for virus treated with AuNP sample coating.

2.8 Statistical analysis

All results are represented as means ± standard deviation of triplicate experiments. Statistical analyses were performed with Student's t-test, with p-value reported as $^*p < 0.05$, $^{**}p < 0.01$, $^{****}p < 0.0001$.

3 Results

3.1 Production and characterisation of PHAs by *P. mendocina* CH50 using unprocessed waste frying oil as the carbon source

20 g/L of the waste frying oil was used as the sole carbon source for the production of PHAs by *P. mendocina* CH50. The temporal profiling of the fermentation process is displayed in Figure 2. The variables monitored throughout the fermentation in the 14 L bioreactor (10 L working volume) were comprised of OD_{450}, pH, DOT %, carbon concentration, nitrogen estimation, and biomass and polymer yield.

During the fermentation, the OD_{450} increased gradually and reached a maximum value of 10.45 at 48 h, indicating sustained bacterial growth until the end of the cultivation. Nitrogen depletion was observed after 6 h. This indicated that a nitrogen-limiting environment was achieved which is essential for the accumulation of PHAs, as described in previous literature (Johnson et al., 2010). The dissolved oxygen tension (DOT%) dropped to 0% after 24 h creating an oxygen-limiting environment for the duration of the fermentation. These nutrient limitations resulted in electron and donor-acceptor fluctuations and caused an increase in the acetyl-CoA/CoA and NAD(P)H/NAD(P+) ratios. This shift in ratios, in turn, inhibited the activity of functional enzymes in the tricarboxylic acid (TCA) cycle and led to the accumulation of intracellular PHAs (Quillaguamán et al., 2010; Moralejo-Gárate et al., 2013; Madhusoodanan et al., 2022). The pH was not controlled during the fermentation process, and it gradually decreased from pH 6.85 to 6.35 after 48 h. This modest acidification can be ascribed to the oxidation of reduced carbon substrates, as previously observed by Sánchez et al. (Sánchez-Clemente et al., 2020). The carbon source was entirely depleted, reaching a final value

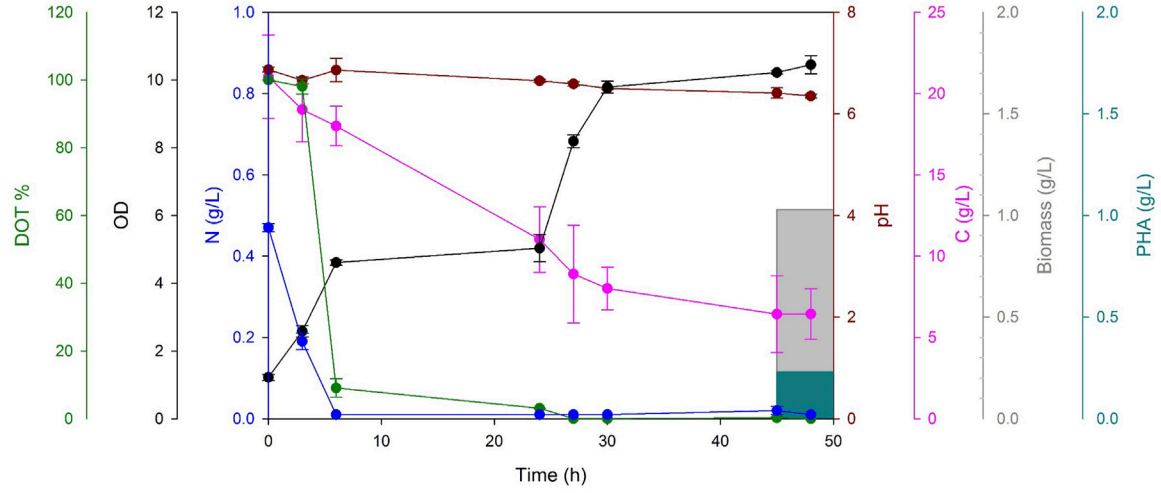

FIGURE 2
Temporal profile of PHA production by *P. mendocina* CH50 using waste frying oil as the sole carbon source. OD_{450}(black line), carbon concentration (g/L, pink line), nitrogen concentration (g/L, blue line), pH (dark red line), dissolved oxygen tension (DOT %, green line), biomass yield (g/L, grey bar), PHA yield (g/L, teal bar).

of 6.44 g/L, and the biomass yield peaked at 1.03 g/L, with the accumulation of 0.23 g/L of polyhydroxyalkanoates (PHAs).

3.1.1 Polymer characterisation

Figure 3A shows a representative picture of the produced PHA, which appeared sticky. Preliminary confirmation of the chemical structure of the produced polymer was conducted through ATR-FTIR. The spectra in Figure 3C showed the presence of two bands, located between 1739 cm^{-1} and 1159 cm^{-1}, corresponding to the ester carbonyl group (C=O) and the acyl group (–CH), respectively. An additional intense peak at 2,920 cm^{-1} corresponding to the stretching vibration of methylene (CH_2) groups was also found. More specifically, the triplet peak located at approximately 2,900 cm^{-1} is assigned the stretching vibration of carbon–hydrogen bond of methyl and methylene group (CH_3, CH_2) (Kann et al., 2014). To determine the monomeric composition of the purified mcl-PHA synthesised by the *P. mendocina* CH50, GC-MS was conducted. The GC-MS chromatograph confirmed that the purified and methanolysed polymers consisted of an mcl-PHA with 5 monomeric units, namely, 3-hydroxyoctainoic acid (3HO), 3hydroxydecanoic acid (3HD) and 3-hydroxydodecanoic acid (3HDD), as shown in Figure 3D. Therefore, the PHA produced by *P. mendocina* CH50 using waste frying oil was P(3HO-co-3HD-co-3HDD). Through GC-MS analysis, the mol% of the monomers were 50 mol% 3HO, 37 mol% 3HD and13 mol% 3HDD. Extra peaks at retention times 8.67 and 9.39 were associated with impurities from the waste frying oil still present in polymer after the purification process. The thermal properties of the PHA were determined from the analysis of the obtained DSC thermogram (Figure 3B). The copolymer showed a glass transition temperature at −36°C which is typical for the MCL-PHAs. The absence of the melting event during the first and the second heating cycles indicated the amorphous nature of the produced polymer indicating that the monomer units were randomly oriented at the molecular level.

3.2 Sustainable biosynthesis and characterisation of gold nanoparticles using *P. mendocina* CH50

We investigated the possibility of synthesizing gold nanoparticles using the cell-free supernatant of the culture of *P. mendocina* CH50 using unprocessed waste frying oil as the carbon source. For the synthesis of gold nanoparticles (AuNPs) hydrogen tetrachloroaurate ($HAuCl_4$) was mixed with cell free supernatant, obtained after 48 h of cultivation. After 24 h of incubation, hydrogen tetrachloroaurate solution treated with the cell-free supernatant changed to reddish colour as shown in Figure 4A. This indicated the occurrence of the redox reaction with the conversion of Au^{3+} ions in the excited state to Au° in the ground state by extracellular compounds present in the supernatant. In contrast to these findings, hydrogen tetrachloroaurate solution without cell free supernatant retained its original colour.

3.2.1 Physicochemical characterisation of the bio fabricated AuNPs

The UV–vis spectrum (Figure 4B) revealed a sharp SPR peak at 530 nm which is a characteristic peak for AuNPs (Husseiny et al., 2007; Rajendran, 2017; Wu and Ng, 2017). There was no corresponding peak at 530 nm in the control solution with AuNPs. The TEM images (Figure 4C) revealed spherical and isolated nanoparticles. The TEM micrographs were used to determine the mean particle size which was calculated to be 3.5 ± 1.5 nm.

The DLS analysis, of the nanoparticles revealed that the average hydrodynamic diameter of the gold nanoparticles in a liquid suspension was 51.3 ± 0.6 nm, which is larger when compared to the TEM data. The higher mean value in DLS analysis could be due to the fact that DLS provides the hydrodynamic radius on an ensemble average (Lim et al., 2013).

10.3389/fnano.2023.1243056

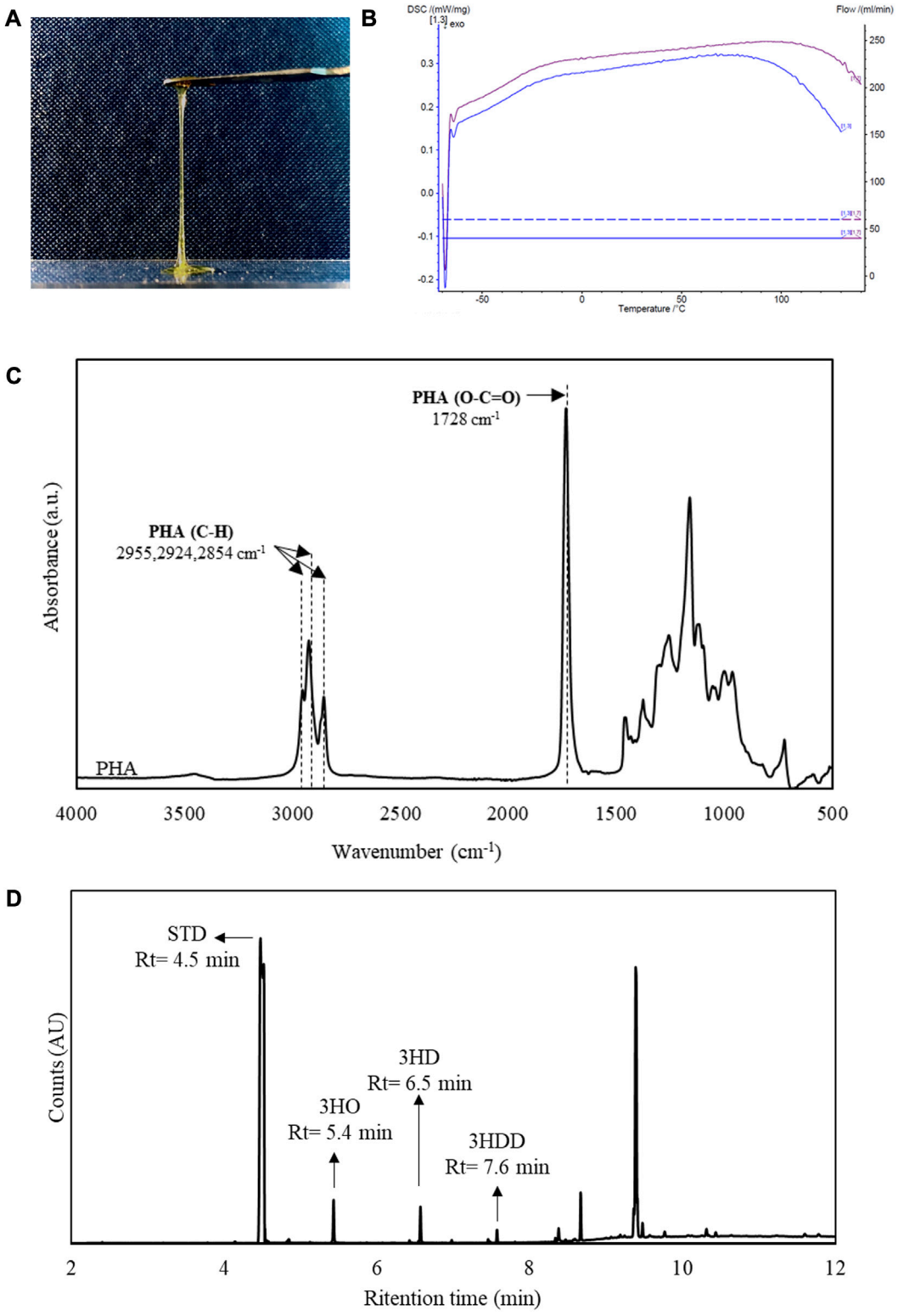

FIGURE 3
(A) Representative picture of PHA produced **(B)** DSC analysis of PHA **(C)** ATR/FTIR spectrum of and **(D)** GC-MS spectra of P(3HO-co-3HD-co-HDD) produced by *P. mendocina* CH50 using waste frying oil as the carbon source. STD = standard, methyl benzoate, 3HO = 3-hydroxyoctainoic acid, methyl ester; 3HD = 3-hydroxydecanoic acid, methyl ester; 3HDD = 3-hydroxydodecanoic acid, methyl ester.

10.3389/fnano.2023.1243056

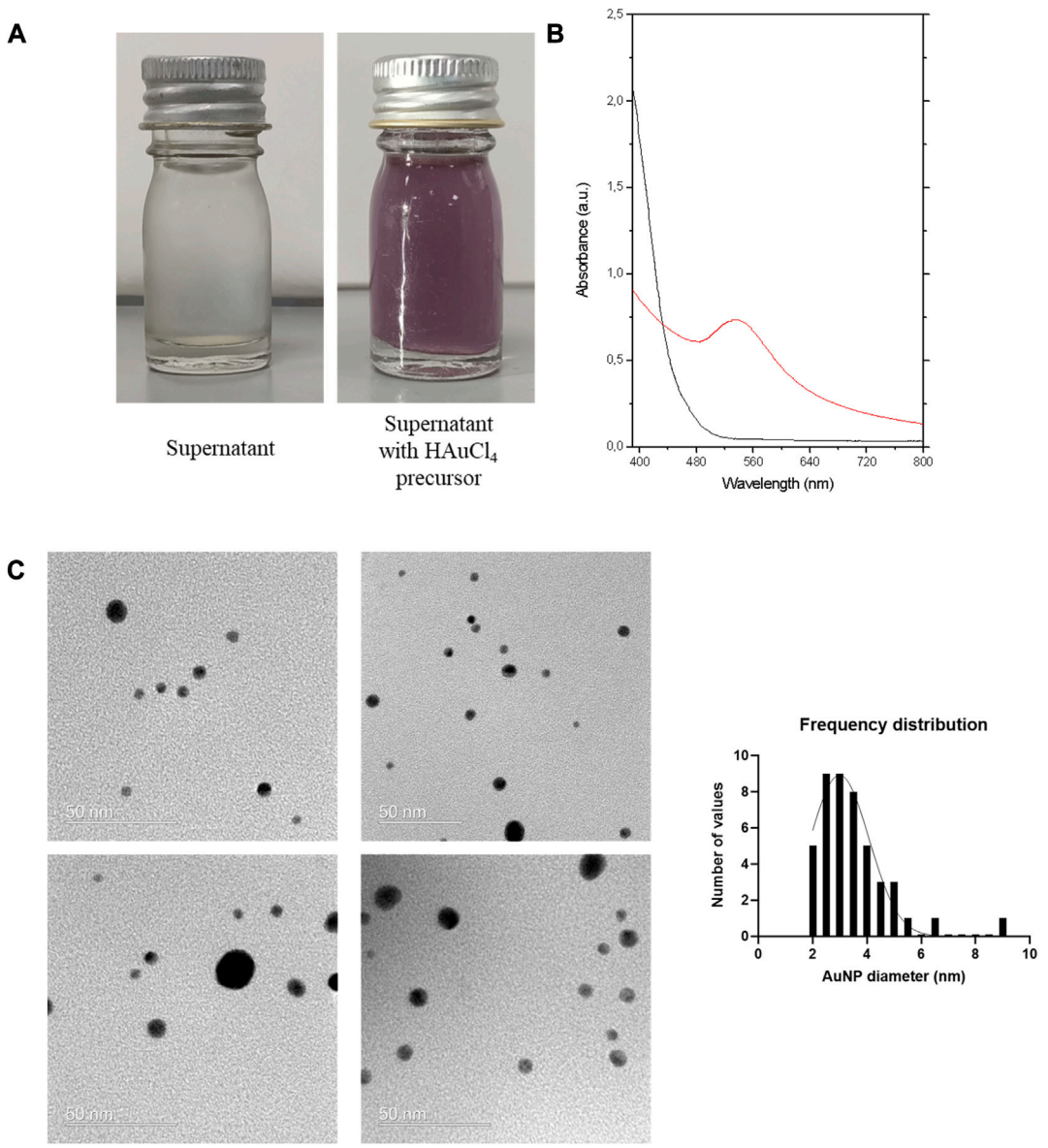

FIGURE 4
(A) Visible observation of biosynthesis of gold nanoparticles (left, no colour change) control solution of nutrient broth containing precursor of $HAuCl_4$ 24 h and (right, reddish colour) solution of cell free supernatant of *P. mendocina* CH50 containing $HAuCl_4$ for 24 h **(B)** UV- visible absorption spectra of 1 mM aqueous gold precursor ($HAuCl_4$) (---), and gold nanoparticles synthesised by cell free supernatant of *P. mendocina* CH50 (---) **(C)** Transmission electron microscopy images of biosynthesised AuNPs with frequency distribution.

3.2.2 Antibacterial and antiviral activity of the biosynthesised AuNPs

3.2.2.1 Antibacterial activity of the biosynthesised fabricated AuNPs

The antibacterial activity of the bio-synthesized AuNPs was tested against Gram–negative (*E. coli* 8739) and Gram-positive (*S. aureus* 6538P) bacteria strains, performing MIC and MBC assays using the broth dilution method. More specifically the AuNPs were inoculated in different concentrations in the presence of the bacterial suspension of *S. aureus* 6538P and *E. coli* 8739 for 24 h respectively. The AuNPs revealed an antibacterial activity against *S. aureus* 6538P with a MIC value of 31.5 μg/mL. MBC values could not be detected. The concentrations of the AuNPs used in the study did not show any antibacterial activity against *E. coli* 8739 indicating that the tested concentrations of AuNPs were not sufficient to inhibit the bacterial growth.

3.2.2.2 Antiviral activity of biosynthesised AuNPs

We investigated the potential of the AuNPs to be used as active antiviral agents against SARS-CoV-2 spike pseudotype virus.

The virucidal activity of the AuNPs was investigated considering the possible application of such materials as components of coatings or biomaterials with antiviral properties. For such an application, the inactivation of virus should occur before contact between the virus and host cells. For this reason, a "pre-treatment" test of the antiviral test was conducted by incubating the virus for 24 h with the AuNPs,

10.3389/fnano.2023.1243056

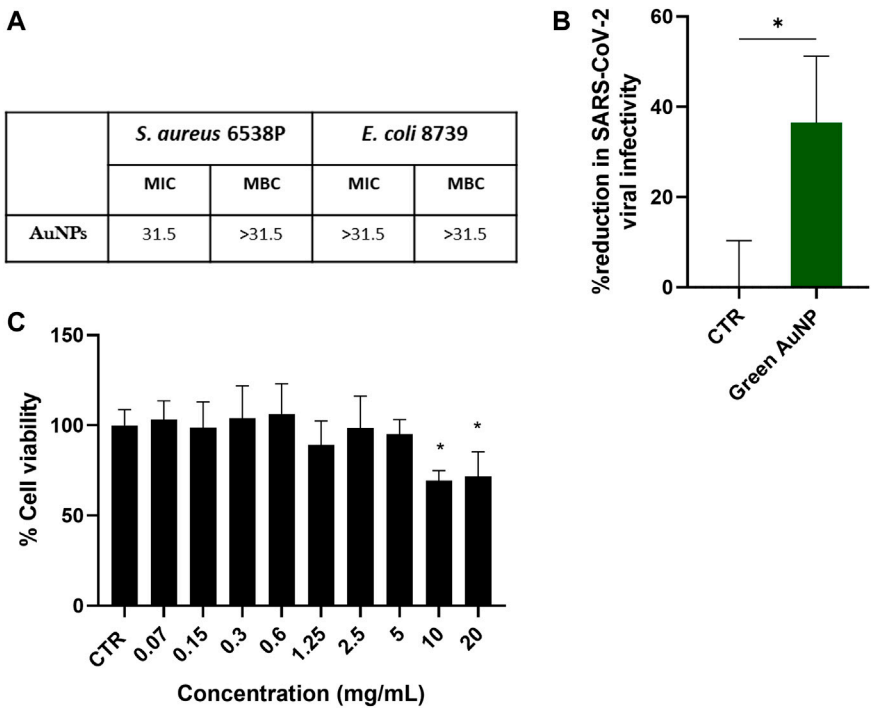

FIGURE 5
(A) MIC and MBC values of AuNPs against *Staphylococcus aureus* 6538P and *Escherichia coli* 8739 **(B)** Antiviral activity of biosynthesised AuNPs (green) against SARS-CoV-2 pseudotype virus. CTR consists of SARS-CoV-2 pseudotype virus incubated with non-treated media. *p-value < 0.5 indicates statistically significant with the CTR (n = 3). **(C)** *In vitro* HEK-293T cells cytocompatibility of AuNPs at different concentrations. CTR refers to cells cultured with non-treated media. *p-value < 0.5 indicates statistically significant with the CTR (n = 3).

to simulate "real life" conditions (such as a surface coating). Then the treated virus was placed in contact with HEK-293T cells that stably express ACE-2 and TMPRSS2 for viral entry and spike protein priming respectively, to evaluate the virucidal effect of AuNPs on SARS-CoV-2 pseudovirus. As shown in Figure 5B an average of 36% reduction in viral infectivity was detected after incubation with AuNPs. These results indicated that at the concentration investigated AuNPs were able to induce a virucidal activity against SARS-CoV-2. To exclude that the antiviral activity could be related to cytotoxicity of the AuNPs, a cytocompatibility study was performed culturing HEK-293T cells in the presence of the compound. As shown in Figure 5C, the AuNPs induced a decrease of cell viability at concentration of 5 and 10 mg/mL, significantly higher than the concentration tested for the antiviral activity, i.e., 1 μg/mL. These results indicated the absence of toxicity of the AuNPs at the concentration investigated.

3.3 Development of coatings based on the combination of P(3HO-co-3HD-co-3HDD-) and biosynthesised AuNPs

Finally, we investigated the potential to combine the products of the dual fermentation process (i.e., PHA and AuNPs) to produce environmentally friendly antibacterial coatings. The coatings were prepared by mixing the produced P(3HO-co-3HD-co-3HDD) (10% w/v) with the AuNPs (10% w/w) in chloroform. The SEM micrographs of the coating combined with the AuNPs (Figure 6B) showed a surface of the biopolymer embedded with different sizes of AuNPs resulting in a non-uniform effect compared to the smooth surface of the biopolymer itself as shown in Figure 6A.

The ATR/FTIR spectra as shown in Figure 6C revealed two prominent peaks located at 3249 and 1627 cm^{-1} in the sample containing the AuNPs corresponding to the stretching vibration of a primary amine (N-H) and the bending vibration of amide (N-H) respectively; implying the presence of biomolecules (proteins/peptides) on the surface of the AuNPs that act as reducing/capping agents and may be responsible for the synthesis of the AuNPs. Such findings have also been previously reported in other studies (Suresh et al., 2011; Shameli et al., 2012; Gurunathan et al., 2014).

Solvent cast films of the produced polymer were prepared as described previously in Basnett et al., 2013. Samples from the produced films were used to measure the hydrophobicity of the PHA films by static water contact angle method. It is acknowledged that the surfaces that present a water contact angle higher than 70° are hydrophobic or water-repellent and they have a low wettability whereas surfaces with contact angles lower than 70° are considered hydrophilic with a high wettability (Peschel et al., 2008; Basnett, 2014). In this light, the produced polymer from WFO with θ value of 88 ± 2.5° are considered to be hydrophobic. The addition of the AuNPs in the polymer matrix via the solvent casting method resulted in a slightly less hydrophobic character of 85.8 ± 3.1° as shown in Figure 6D.

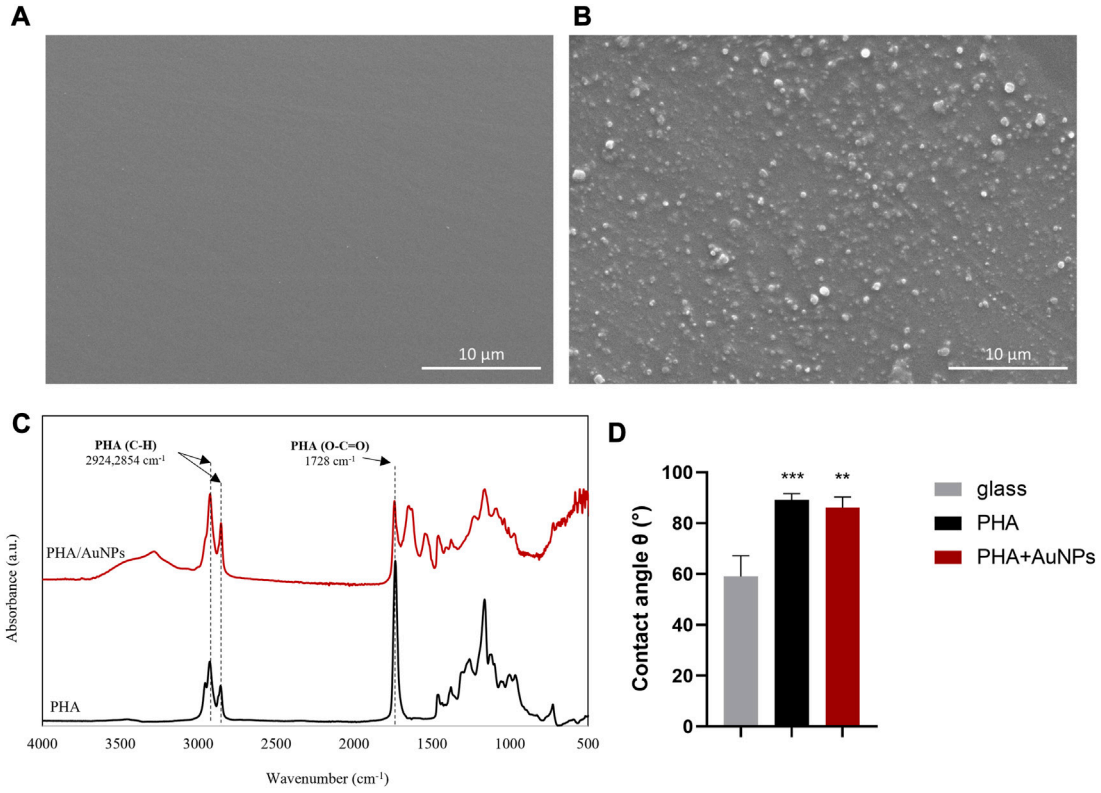

FIGURE 6
(A,B) SEM images **(C)** ATR/FTIR spectra of a P(3HO-co-3HD-co-3HDD-) and the blend of P(3HO-co-3HD-co-3HDD-) with, AuNPs, **(D)** Static water contact angle measurement of glass slide (grey), P(3HO-co-3HD-co-3HDD-) (black) and the P(3HO-co-3HD-co-3HDD-) containing AuNPs (red). $^{**}p$-value < 0.01 indicates statistically significant with the glass slide (n = 3).

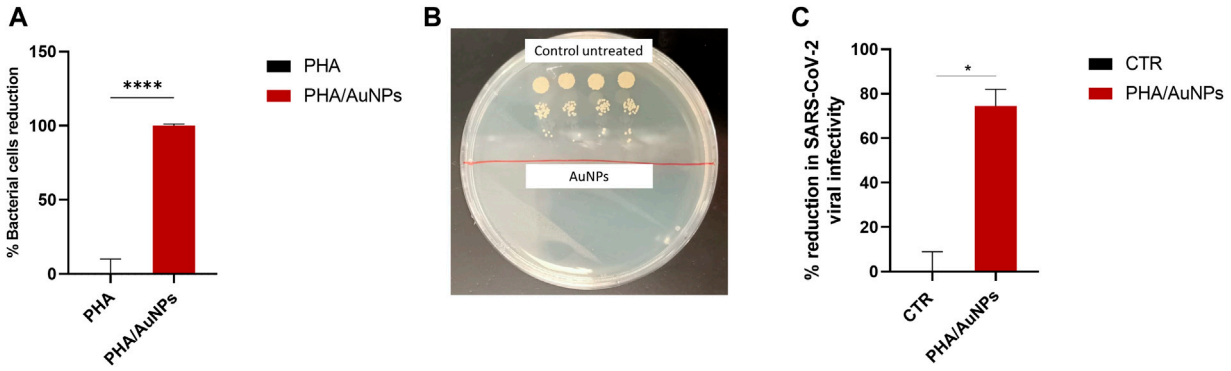

FIGURE 7
(A) Antibacterial activity (ISO 22196) of PHA and PHA/AuNPs against coatings against *Staphylococcus aureus* 6538P. $^{****}p$-value < 0.0001 indicates statistically significant difference between the composite film and neat film (n = 3). **(B)** Examplary image of colony formin unit (CFU) of ISO 22196 for the control (untread sample) and for AuNPs. **(C)** Antiviral activity of PHA/AuNP coatings CTR consists of SARS-CoV-2 pseudotype virus incubated with non-treated media. $^{*}p$-value < 0.05 indicates statistically significant difference between the composite film and CTR (n = 3).

3.3.1 Antibacterial and antiviral activity of AuNPs/PHAs coatings

3.3.1.1 Antibacterial activity of the AuNPs/PHA coatings—ISO 22196

ISO 22196 was performed to investigate the antimicrobial activity of the AuNPs against *S. aureus* 6538P, seeded directly on to the surface of the materials. AuNPs loaded within P(3HO-co-3HD-co-3HDD-co-3HHD-co-3HOD) films showed to be active against the bacterial species at loading content investigated, inducing a reduction of the bacterial cell number as compared to the respective neat samples. The materials showed a high efficacy, causing a 100% killing of *S. aureus* 6538P Figures 7A and B. No antibacterial activity could be detected for the coatings without AuNPs.

3.3.1.2 Antiviral activity of the AuNPs/PHA coatings

Antiviral activity of the PHA/AuNPs coatings was investigated by exposing the coated surfaces to SARS-CoV-2 virus for 24 h. After the incubation time, virus was then harvested and used to infect HEK293T(+ACE2+TMPRSS2) target cells. The virucidal activity was tested evaluating the luciferase activity of the treated and untreated samples. The developed coatings based on the mixture of P(3HO-co-3HD-co-3HDD-) and AuNPs showed a high virucidal activity, inducing an average 75% reduction in viral infectivity, compared to the virus control, and the difference was statistically significant (Figure 7C).

4 Discussion

In this study, we successfully developed a novel, sustainable, and cost-effective process to produce a bio-based coating with antibacterial and antiviral properties. Our approach involved incorporating AuNPs within a PHA matrix. The key innovation of our work is the utilisation of *P. mendocina* CH50 for both extracellular biosynthesis of AuNPs and the intracellular production of the PHA matrix.

As previously stated, *P. mendocina* CH50 was also employed for intracellular production of PHAs. To enhance the sustainability of biopolymer production, waste frying oil was used as a low-cost carbon source for PHA production resulting in 1.03 g/L of biomass, accumulating 0.23 g/L of PHA over a period of 48 h, yielding a final 22% of dried cell weight (% dcw) This specific strain has already been investigated as a PHA producer using both related and unrelated carbon substrates. The use of pure fatty acids (i.e., sodium octanoate) or a mixture of fatty acid (i.e., coconut oil) led to the production of semicrystalline PHAs by *P. mendocina* CH50 with a yield 31% and 58% dcw respectively (Rai et al., 2011; Basnet et al., 2018). In the presence of unrelated substrates, a 39.5% of accumulation was obtained when the strain was cultivated with biodiesel waste, while sugarcane molasses led to a 14.22% dcw accumulation (Basnett et al., 2017; Basnett et al., 2020). Overall, several other authors have reported the use of *Pseudomonas* species as the bacterial host and frying oil as the carbon source (even combined with other substrates), yielding 6.45%–42.6% of PHAs content (Rai et al., 2011; Możejko-Ciesielska and Kiewisz, 2016). For instance, Mozejko and co-workers, reported the production of PHAs using *Pseudomonas* Gl01 strain in a two-step fed-batch fermentation using glucose and waste rapeseed oil as carbon sources, thereby yielding 3.0 g/L of CDW with 20% of PHAs content within 48 h of cultivation. Another study utilised *Pseudomonas chlororaphis* 555 in a fed-batch fermentation mode, employing waste cooking oil as the sole carbon source. This resulted in a biomass accumulation of 13.9 g/L and a PHA volumetric productivity of 0.29 g/L/h. Additionally, Song et al. (2008) demonstrated that *Pseudomonas* sp. strain DR2 was capable of accumulating mcl-PHAs using waste vegetable oil as the sole carbon source. Compared to the existing literature, our study highlights the potential of *P. mendocina* CH50 as a promising PHA-producer strain from waste frying oil. However, future research should focus on enhancing its PHA productivity. Several strategies could be investigated in future work based on literature approaches to increase both biomass and PHA accumulation: saponification (Możejko and Ciesielski, 2013; Ruiz et al., 2019a) of the waste frying oil to improve its aqueous solubility, investigation of advanced culture conditions (e.g., fed-batch or continuous fermentation (Blunt et al., 2018; Ruiz et al., 2019b) and engineering bacterial (Favaro et al., 2018; Ganesh Saratale et al., 2021) strains to achieve more efficient PHAs production.

PHA produced in this study was a long chain-length material, consisted with 3 monomeric units (3HO), (3HD) and (3HDD) ((P(3HO-co-3HD-co-3HDD))). It exhibited an elastomeric, sticky form at room temperature, with a low glass transition temperature of −36°C. It lacked a melting event, indicating its amorphous nature, where the monomer units were randomly oriented at the molecular level. Similar findings were reported by Basnett et al., where the absence of the melting event was associated with the amorphous nature of the P(3HHx-co-3HO-co-3HD-co-3HDD), from *P. mendocina* CH50 cultivated using unprocessed biodiesel waste. Moreover, C. Ruiz, et al. (2019a) have found that the accumulated PHA using WFO as the substrate for the *P. chlororaphis* 555 did not possess any melting event and showed a very low glass transition temperature, indicating a completely amorphous polymer (Ruiz et al., 2019a). The PHA extracted from *P. resinovonas* utilising soyabean oil as the carbon substrate showed a glass transition temperature of −45°C with no melting transition observed, stipulating the amorphous state of the produced PHA (Ashby and Foglia, 1998). Song *et al.* (2008) also reported the amorphous production of MCL-PHA using as producer *Pseudomonas* sp. strain DR2 utilizing waste vegetable oil. The amorphous nature of the produced polymer was ascribed to the presence of the long aliphatic chains which hinder the arrangement at the molecular level and hence the crystallinity of the final polymer (Song et al., 2008). The hydrophobic nature of the PHA produced from waste frying oil aligns with the data in the literature, where MCL-PHAs have shown hydrophobic behavior with water contact angles ranging from 77 to 104° (Rai et al., 2011; Bagdadi et al., 2018). The hydrophobicity of the MCL-PHAs is ascribed to the presence of the long alkyl pendant groups in the side chains of the polymer backbone (Menzies and Jones, 2010).

Another sustainable feature of our study was the biological production of AuNPs by utilising a cell-free bacterial supernatant, which is typically discarded after PHA extraction. Specifically, the proteins within the supernatant acted as capping and reducing agent of $HAuCl_4$ solution for the formation of the nanoparticles. This biological synthesis of AuNPs follows a bottom-up approach, resulting in the formation of morphologically uniform nanoparticles with distinct physical, chemical, electrical, mechanical, thermal, optical, and biological properties (Okkeh et al., 2021; Suriyakala et al., 2022). Several microorganisms have been reported as potential biological sources for extracellular AuNPs production, utilising reducing agents present in their cultivation supernatant. For instance, Mewada et al. demonstrated that NADPH-dependent enzymes secreted by species like *Pseudomonas denitrificans* and *Rhodopseudomonas capsulate*, can reduce Au^{3+} ions to Au^0 (Mewada et al., 2012).

The formation of AuNPs was initially observed by visual inspection as the colour of the precursor hydrogen tetrachloroaurate ($HAuCl_4$) changed from yellow/off-white to reddish colour, after 24 h of the reaction, when the final concentration of gold ions reached 1 mM. This was further confirmed by the UV-Vis spectrum, which exhibited a distinct and broad surface plasmon resonance (SPR) peak at 530 nm, indicating the presence of fabricated AuNPs (Yallappa et al., 2013; Suvarna et al., 2017). Moreover, the FTIR analysis showed the functional groups of the proteinaceous material, that acted as capping/stabilizing agent binding the AuNPs either through free

amine groups or cysteine residues (Nichols et al., 2009; Suresh et al., 2011; Gurunathan et al., 2014). The bands at 2855 and 2960 cm^{-1} could be assigned to the C–H stretching where the bands located at 3303, 1735 and 1231 cm^{-1} correspond to carbonyl and hydroxyl functional groups in alcohols and phenol derivatives (Suresh et al., 2011; Gurunathan et al., 2014). These findings align with previous studies on biosynthesised nanoparticles (Shameli et al., 2012; Suresh et al., 2010; Suresh et al., 2011; Gurunathan et al., 2014). Furthermore, TEM analysis provided direct visualisation of the spherical shape and size (average diameter of 3.5 nm) of the synthesised nanoparticles. Spherical MNPs with small diameter are known to be less cytotoxic in nature. A previous study conducted by Enea et al., demonstrated that sphere-shaped AuNPs exhibit lower toxicity compared to star-shaped ones (Enea et al., 2019). Also, larger AuNPs with 50 nm were more cytotoxic. Recent studies have focused on the development of sub-5 nm nanoparticles to enhance their delivery, biocompatibility, and pharmacokinetics (Leifert et al., 2013; Kim et al., 2020). Considering this, the AuNPs obtained in this study hold great potential as a sustainable tool for addressing current challenges in medical applications. They can be explored for their efficacy as antiviral agents, imaging and theragnostic properties. Furthermore, their slow clearance may alleviate safety concerns associated with synthetic nanoparticle usage (Xie et al., 2020).

The difference between TEM and DLS analysis is ascribed to the interference of the dispersant into the hydrodynamic diameter where forces such as van der Waals interaction in the solution tends to increase the particle size in the liquid sample analysed by DLS. Additionally, the variation in size distribution of the nanoparticles is more evident in DLS analysis when the sample is polydispersed compared to TEM analysis. Other studies have also reported similar dilemma when analysing gold nanoparticles with TEM and DLS (Suresh et al., 2011; Gurunathan et al., 2014; Fischer and Schmidt, 2016; Souza et al., 2016; El-Batal et al., 2019). Additionally, the DLS measurements in our case was conducted without the addition of any surfactant and hence this might be one of the reasons of the noticeable difference of the measurements between TEM and DLS analysis. Usually, surfactants are used in DLS measurements to stabilise and prevent agglomeration of nanoparticles. The need for surfactants depends on the synthesis method and the natural stabilizing agents present in the colloidal solution (Pallipurath et al., 2014). TEM provides direct imaging of individual nanoparticles and allows researchers to visualise the size, shape, and morphology of the AuNPs with high resolution.

Conventionally synthesised AuNPs have been achieved using different chemicals routes such as Brust-Schiffrin, Turkevich and Martin method. Chemicals such as ascorbic acid, sodium citrate, sodium borohydride and others have been used to reduce the precursor of $HAuCl_4$ to AuNPs (Teimouri et al., 2018; Daruich De Souza et al., 2019; Riberio da Cuncha et al., 2019; Hammami et al., 2021). In a UV-assisted synthesis of AuNPs, it was revealed that after 10 min of UV irradiation the obtained mixture had a pink colour and the SPR was detected at 526 nm indicating the reduction of the precursor aqueous solutions of $HAuCl_4$ (Gomes et al., 2023). The TEM measurement revealed the obtained spherical particles to be between 12–18 nm. In another study, L-ascorbic acid was used as a reducing agent following a modified Turkevich approach which resulted in spherical nanoparticles ranging from 9.7 to 13.9 nm in 20% and 50% volumetric percentage of ethanol to water solvent mixture respectively. The SPR was detected at 514 nm and 520 nm respectively conforming the production of AuNPs in a low volume percentage of ethanol (Hussain et al., 2020). In a separate study, reducing agent tetrabutylammonium borohydride ($TBABH_4$) solubilised in ethylene glycol (EG) and toluene using a modified Brust–Schiffrin method resulted in the production of hydrophobic AuNPs. The TEM analysis showed spherical particles ranging from 8–13 nm depending on the concentration of reducing agent. The SPR spectra was detected around 520 nm validating the reduction of $HAuCl_4$ (Distaso and Peukert, 2023). The AuNPs produced in this study, via an alternative route, were found to be 3.5 nm in diameter based on the TEM measurements and the SPR was detected at 530 nm. The values are comparable to the aforementioned approaches of producing gold nanoparticles via traditional chemical and physical methods.

These AuNPs were successfully tested as antimicrobial and biocidal agents. Previous studies have explored the activity of AuNPs obtained through chemical or more sustainable synthesis processes, demonstrating a broad spectrum of efficacy against bacterial cells (Zhang et al., 2015; Su et al., 2020). The effectiveness of these nanoparticles depends on their concentration, which can range from a few μg/mL to hundreds of μg/mL, as well as the physicochemical properties influenced by the synthesis method (Okkeh et al., 2021; Piktel et al., 2021). In our study, we evaluated the antibacterial activity of the AuNPs against *Staphylococcus aureus* 6538P (a Gram-positive bacterium) and *Escherichia coli* 8739 (a Gram-negative bacterium). The AuNPs demonstrated antibacterial activity against *S. aureus* 6538P, with a minimum inhibitory concentration (MIC) of 31.5 μg/mL. However, no minimum bactericidal concentration (MBC) was detected within the range of concentrations investigated. These results indicated that at these concentrations the material showed a bacteriostatic rather than bactericidal effect. On the other hand, no antibacterial activity could be detected against *E. coli* 8739, as the nanoparticles did not induce a reduction of the bacterial growth at the concentrations analysed. The differences observed in the antibacterial activity could be ascribed to their interaction with the microorganisms which depends on the shape, size, surface charge and functionalisation of the materials (Shamaila et al., 2016; Okkeh et al., 2021). Specifically, Piktel et al. showed a higher killing percentage of non-spherical AuNP (e.g., rod shape, star shape) compared to spherical ones, associated with a higher capability of inducing membrane permeabilization leading to bacterial death. If such mechanism is considered the predominant mode of action of AuNPs, the antibacterial activity results obtained in this study could be associated with the intrinsic differences in composition of the structure of the bacterial cell wall between Gram-positive and negative species, making the latter usually less susceptible to the action of harmful molecules (Breijyeh et al., 2020).

Recent studies have reported that AuNPs also exhibit antiviral properties. The antiviral activity of the AuNPs applies to several viruses including herpes virus, influenza, adenovirus, severe acute respiratory syndromes (SARS), rotavirus and others. The effectivity of the antiviral action is ascribed to several different parameters such as the shape and size of the AuNPs, which attach and enter the viral envelope, resulting in the reduction of viral replication. Additionally, other studies report cleavage of the disulfide bonds by the AuNPs and hence block the virus fusion and entry to the host cell membrane. One of the studies reported that the AuNPs reduced cytopathic effect (CPE) of HSV-1 in Vero cells in a size, shape, dose- and time-dependent manner, with the strongest antiviral activity demonstrated by the AuNPs of lower diameter. In another *in vitro*

antiviral study, inhibition of influenza virus infection was achieved in the presence of as low as 0.06 μg/mL AuNPs and advanced in a dose-dependent manner. A remarkable decrease in viral infectivity was observed by Kim et al., when porous AuNPs seeded in cultures of MDCK cells exposed to various IV strains (H1N1, H3N2, and H9N2) (Kim et al., 2020). A 42.75% reduction in infectivity of Herpes Simplex virus (HSV-1) in the presence of 31.25 μL of AuNPs was reported by El-Sheekh et al. (El-Sheekh et al., 2020). Another study found that the conjugation of biocompatible polymers with AuNPs possessed antiviral activity against HIV-1 and influenza virus (subtypes: H1N1, H3N2, H5N1). Inhibition of attachment of influenza virus H1N1 was reported by Papp et al., when modified AuNPs were coated with sialic acid (SA) (Papp et al., 2010).

In this study we investigated the antiviral activity of the AuNPs against SARS-CoV-2 pseudovirus and have shown a significant reduction in viral infectivity compared to untreated virus. These AuNPs could potentially be used as a surface coating commercially in a hospital setting where patients and staff might be shedding virus and reduce fomite transmission of the virus. Scientists have found that SARS-CoV-2 was detectable in aerosols for up to 3 h, up to 4 h on copper, up to 24 h on cardboard and 2–3 days on plastic and stainless steel, and people can acquire the virus not only by aerosol transmission but touching contaminated objects National Institutes of Health (2020) (National Institutes of Health, 2020; van Doremalen et al., 2020). In future, the stability of the obtained AuNPs at various time periods will be measured using UV-Vis spectroscopy, DLS and TEM techniques (Borse and Konwar, 2020; Holišová et al., 2021; Locarno et al., 2021).

Finally, the combination of the eco-friendly AuNPs with PHA produced by *P. mendocina* CH50 cultivated using waste frying oil led to the development of a sustainable, cost-effective coating. This coating was first characterised for its physicochemical properties which revealed a non-homogenous surface of sample with varied sizes of AuNPs deposited on the surface. Additionally, the coating surface exhibited a slightly less hydrophobic nature compared to the surface of the non-coated PHA, which is consistent with previous findings reported by Sengupta and Prasad (Sengupta and Prasad, 2018). In future a more in-depth characterisation of the surface properties of the AuNPs/PHA coating could be conducted using Atomic Force Microscopy (Bagatella et al., 2022; Pospisilova et al., 2022). The potential of these composite materials as coatings with antibacterial and antiviral properties was also investigated. The persistence of viruses on surfaces can vary depending on surface properties such as hydrophobicity, porosity, and roughness, as well as environmental conditions and the presence of other microorganisms or biofilms that can enhance virus survival (Rakowska et al., 2021). These coatings could be particularly useful in hospital environments to reduce the potential transmission of pathogens through contaminated surfaces (fomite transmission). In this study, the composite coating showed high antibacterial activity, inducing 100% bactericidal activity against *S. aureus* 6538P. Further investigations will be conducted to explore the potential of these materials in discouraging biofilm formation. In relation to the antiviral activity, we investigated the possibility of the composite materials to induce inactivation of the virus through incubation over a 24 h period. The AuNP/PHA composite coatings showed significant antiviral activity, by inducing a 75% reduction in virus infectivity. Further investigation of the antimicrobial properties of these coatings will be ascertained during a range of different incubation times. Moreover, the antiviral activity of these composite coatings will be evaluated against different variants of SARS-CoV-2 in circulation, focusing in particular on variants of concern (VoC).

5 Conclusion

In this work we demonstrate a sustainable, and cost-effective method for the synthesis of AuNPs and PHA production by *P. mendocina* CH50 using waste frying oil as the sole carbon source. An amorphous, long chain PHA (P(3HO-co-3HD-co-3HDD)) with hydrophobic properties was produced. Extracellular production of spherical AuNPs with a diameter of 3.5 nm was confirmed by UV-vis, FTIR, and TEM analysis. The obtained AuNPs displayed both antibacterial and antiviral activity. The developed biobased coating of the PHA and the AuNPs was also investigated for its physicochemical properties and demonstrated antibacterial and antiviral activity.

Data availability statement

The original contributions presented in the study are included in the article/Supplementary material, further inquiries can be directed to the corresponding authors.

Author contributions

EM and AP contributed to the research and investigation process and wrote the initial draft of the manuscript. EM, AP, VV, and LE performed the experiments, data collection, and data analysis. EW provided the SARS-CoV-2 spike pseudotype virus and AM performed the antiviral screening assays. PB, AM, and BN contributed to study conceptualization, validation supervision, project administration, and funding acquisition. All authors contributed to the article and approved the submitted version.

Funding

This research was funded by the Health Innovation and Wellbeing community, University of Westminster.

Acknowledgments

The authors would like to thank the technical team at the School of Life Sciences, University of Westminster for their assistance with the laboratory-based research. They would also like to thank the Institute of Archaeology, University College London for the help with the SEM analysis.

Conflict of interest

The authors declare that the research was conducted in the absence of any commercial or financial relationships that could be construed as a potential conflict of interest.

Publisher's note

References

Pospisilova, Aneta, Vodicka, J., Trudicova, M., Juglova, Zuzana, Smilek, J., Mencik, Premysl, et al. (2022). Effects of differing monomer compositions on properties of P(3HB-co-4HB) synthesized by aneurinibacillus sp. H1 for various applications. *Polymers* 14 (10), 2007. doi:10.3390/polym14102007

Anik, M. I., Mahmud, N., Al Masud, A., and Hasan, M. (2021). Gold nanoparticles (GNPs) in biomedical and clinical applications: a review. *Nano Sel.* 3 (4). doi:10.1002/nano.202100255

Ashby, R. D., and Foglia, T. A. (1998). Poly(hydroxyalkanoate) biosynthesis from triglyceride substrates. *Appl. Microbiol. Biotechnol.* 49 (4), 431–437. doi:10.1007/s002530051194

Bagatella, S., Ciapponi, R., and Turri, S. (2022). Nanomechanical characterization of bacterial polyhydroxyalkanoates using atomic force microscopy. *Appl. Sci.* 12 (10), 4994. doi:10.3390/app12104994

Bagdadi, A. V., Safari, M., Dubey, P., Basnett, P., Sofokleous, P., Humphrey, E., et al. (2017). Poly(3-hydroxyoctanoate), a promising new material for cardiac tissue engineering. *J. Tissue Eng. Regen. Med.* 12 (1), e495–e512. doi:10.1002/term.2318

Barber, S., and Sutherland, N. (2017). DEBATE PACK O'neill review into antibiotic resistance. Available at: https://researchbriefings.files.parliament.uk/documents/CDP-2017-0074/CDP-2017-0074.pdf.

Basnett, P., Ching, K. Y., Stolz, M., Knowles, J. C., Boccaccini, A. R., Smith, C., et al. (2013). Novel Poly(3-hydroxyoctanoate)/Poly(3-hydroxybutyrate) blends for medical applications. *React. Funct. Polym.* 73 (10), 1340–1348. doi:10.1016/j.reactfunctpolym.2013.03.019

Basnett, P., Lukasiewicz, B., Marcello, E., Gura, H. K., Knowles, J. C., and Roy, I. (2017). Production of a novel medium chain length poly(3-hydroxyalkanoate) using unprocessed biodiesel waste and its evaluation as a tissue engineering scaffold. *Microb. Biotechnol.* 10 (6), 1384–1399. doi:10.1111/1751-7915.12782

Basnett, P., Marcello, E., Lukasiewicz, B., Nigmatullin, R., Paxinou, A., Ahmad, M. H., et al. (2020). Antimicrobial materials with lime oil and a poly(3-hydroxyalkanoate) produced via valorisation of sugar cane molasses. *J. Funct. Biomaterials* 11 (2), 24. doi:10.3390/jfb11020024

Basnett, P., Marcello, E., Lukasiewicz, B., Panchal, B., Nigmatullin, R., Knowles, J. C., et al. (2018). Biosynthesis and characterization of a novel, biocompatible medium chain length polyhydroxyalkanoate by Pseudomonas mendocina CH50 using coconut oil as the carbon source. *J. Mater. Sci. Mater. Med.* 29 (12), 179. doi:10.1007/s10856-018-6183-9

Basnett, P. (2014). WestminsterResearch Biosynthesis of polyhydroxyalkanoates, their novel blends and composites for biomedical applications. Available at: https://westminsterresearch.westminster.ac.uk/download/24e5cf811f3b6a91e42e89a01ca23146a142fe21ab556388bce4955ca7dee378/5912392/Pooja_BASNETT_2014.pdf.

Blunt, W., Levin, D., and Cicek, N. (2018). Bioreactor operating strategies for improved polyhydroxyalkanoate (PHA) productivity. *Polymers* 10 (11), 1197. doi:10.3390/polym10111197

Borse, V., and Konwar, A. N. (2020). Synthesis and characterization of gold nanoparticles as a sensing tool for the lateral flow immunoassay development. *Sensors Int.* 1, 100051. doi:10.1016/j.sintl.2020.100051

Breijyeh, Z., Jubeh, B., and Karaman, R. (2020). Resistance of gram-negative bacteria to current antibacterial agents and approaches to resolve it. *Molecules* 25 (6), 1340. doi:10.3390/molecules25061340

Carnell, G. W., Ferrara, F., Grehan, K., Thompson, C. P., and Temperton, N. J. (2015). Pseudotype-based neutralization assays for influenza: A systematic analysis. *Front. Immunol.* 6, 161. doi:10.3389/fimmu.2015.00161

Chen, P., Song, L., Liu, Y., and Fang, Y. (2007). Synthesis of silver nanoparticles by γ-ray irradiation in acetic water solution containing chitosan. *Radiat. Phys. Chem.* 76 (7), 1165–1168. doi:10.1016/j.radphyschem.2006.11.012

Daruich De Souza, C., Ribeiro Nogueira, B., and Rostelato, M. E. C. M. (2019). Review of the methodologies used in the synthesis gold nanoparticles by chemical reduction. *J. Alloys Compd.* 798, 714–740. doi:10.1016/j.jallcom.2019.05.153

Dickey, S. W., Cheung, G. Y. C., and Otto, M. (2017). Different drugs for bad bugs: antivirulence strategies in the age of antibiotic resistance. *Nat. Rev. Drug Discov.* 16 (7), 457–471. doi:10.1038/nrd.2017.23

Dinjaski, N., Fernández-Gutiérrez, Mar, Selvam, Shivaram, Parra-Ruiz, F. J., Lehman, S., San Román, Julio, García, E., José Luis García, García, A. J., and Prieto, María Auxiliadora (2014). PHACOS, a functionalized bacterial polyester with bactericidal activity against methicillin-resistant *Staphylococcus aureus*. *Biomaterials* 35 (1), 14–24. doi:10.1016/j.biomaterials.2013.09.059

Distaso, M., and Peukert, W. (2023). A biphasic batch and continuous flow synthesis of hydrophobic gold and silver nanoparticles. *React. Chem. Eng.* 8. doi:10.1039/D3RE00132F

El-Batal, A. I., Al-Hazmi, N. E., Mosallam, F. M., and Elsayed, M. A. (2018). Biogenic synthesis of copper nanoparticles by natural polysaccharides and Pleurotus ostreatus fermented fenugreek using gamma rays with antioxidant and antimicrobial potential towards some wound pathogens. *Microb. Pathog.* 118, 159–169. doi:10.1016/j.micpath.2018.03.013

El-Sheekh, M. M., Shabaan, M. T., Hassan, L., and Morsi, H. H. (2020). Antiviral activity of algae biosynthesized silver and gold nanoparticles against Herps Simplex (HSV-1) virus *in vitro* using cell-line culture technique. *Int. J. Environ. Health Res.* 32 (2), 616–627. doi:10.1080/09603123.2020.1789946

Enea, M., Vale, M., Eaton, P., Silva, D., Pereira, E., Júlia, M., et al. (2019). A multiparametric study of gold nanoparticles cytotoxicity, internalization and permeability using an*in vitro*model of blood–brain barrier. Influence of size, shape and capping agent. *Nanotoxicology* 13 (7), 990–1004. doi:10.1080/17435390.2019.1621398

Favaro, L., Basaglia, M., and Casella, S. (2018). Improving polyhydroxyalkanoate production from inexpensive carbon sources by genetic approaches: A review. *Biofuels, Bioprod. Biorefining* 13 (1), 208–227. doi:10.1002/bbb.1944

Fernández, D., Rodríguez, E., Bassas, M., Viñas, M., Solanas, A. M., Llorens, J., et al. (2005). Agro-industrial oily wastes as substrates for PHA production by the new strain *Pseudomonas aeruginosa* NCIB 40045: effect of culture conditions. *Biochem. Eng. J.* 26 (2-3), 159–167. doi:10.1016/j.bej.2005.04.022

Fischer, K., and Schmidt, M. (2016). Pitfalls and novel applications of particle sizing by dynamic light scattering. *Biomaterials* 98, 79–91. doi:10.1016/j.biomaterials.2016.05.003

Ganesh Saratale, R., Cho, S.-K., Dattatraya Saratale, G., Kadam, A. A., Ghodake, G. S., Kumar, M., et al. (2021). A comprehensive overview and recent advances on polyhydroxyalkanoates (PHA) production using various organic waste streams. *Bioresour. Technol.* 325, 124685. doi:10.1016/j.biortech.2021.124685

Gomes, D. S. B., Paterno, L. G., Santos, A. B. S., Barbosa, D. P. P., Holtz, B. M., Souza, M. R., et al. (2023). UV-accelerated synthesis of gold nanoparticle–pluronic nanocomposites for X-ray computed tomography contrast enhancement. *Polymers* 15 (9), 2163. doi:10.3390/polym15092163

Gurunathan, S., Han, J., Park, J. H., and Kim, J.-H. (2014). A green chemistry approach for synthesizing biocompatible gold nanoparticles. *Nanoscale Res. Lett.* 9 (1), 248. doi:10.1186/1556-276x-9-248

Haba, E., Vidal-Mas, J., Bassas, M., Espuny, M. J., Llorens, J., and Manresa, A. (2007). Poly 3-(hydroxyalkanoates) produced from oily substrates by *Pseudomonas aeruginosa* 47T2 (NCBIM 40044): effect of nutrients and incubation temperature on polymer composition. *Biochem. Eng. J.* 35 (2), 99–106. doi:10.1016/j.bej.2006.11.021

Hammami, I., Alabdallah, N. M., jomaa, A. A., and kamoun, M. (2021). Gold nanoparticles: synthesis properties and applications. *J. King Saud Univ. - Sci.* 33 (7), 101560. doi:10.1016/j.jksus.2021.101560

Herigstad, B., Hamilton, M., and Heersink, J. (2001). How to optimize the drop plate method for enumerating bacteria. *J. Microbiol. Methods* 44 (2), 121–129. doi:10.1016/s0167-7012(00)00241-4

Holišová, V., Urban, M., Konvičková, Z., Kolenčík, M., Mančík, P., Slabotinský, J., et al. (2021). Colloidal stability of phytosynthesised gold nanoparticles and their catalytic effects for nerve agent degradation. *Sci. Rep.* 11 (1), 4071. doi:10.1038/s41598-021-83460-1

Hussain, M. H., Abu Bakar, N. F., Mustapa, A. N., Low, K.-F., Othman, N. H., and Adam, F. (2020). Synthesis of various size gold nanoparticles by chemical reduction method with different solvent polarity. *Nanoscale Res. Lett.* 15 (1), 140. doi:10.1186/s11671-020-03370-5

Husseiny, M. I., El-Aziz, M. A., Badr, Y., and Mahmoud, M. A. (2007). Biosynthesis of gold nanoparticles using *Pseudomonas aeruginosa*. *Spectrochimica Acta. Part A, Mol. Biomol. Spectrosc.* 67 (3-4), 1003–1006. doi:10.1016/j.saa.2006.09.028

Wu, Jhe Ming, and Ng, I-Son (2017). Biofabrication of gold nanoparticles by Shewanella species. *Bioresour. Bioprocess.* 4 (1), 50. doi:10.1186/s40643-017-0181-5

Johnson, K., Kleerebezem, R., and van Loosdrecht, M. C. M. (2010). Influence of the C/N ratio on the performance of polyhydroxybutyrate (PHB) producing sequencing

batch reactors at short SRTs. *Water Res.* 44 (7), 2141–2152. doi:10.1016/j.watres.2009.12.031

Kann, Y., Shurgalin, M., and Krishnaswamy, R. K. (2014). FTIR spectroscopy for analysis of crystallinity of poly(3-hydroxybutyrate-co-4 -hydroxybutyrate) polymers and its utilization in evaluation of aging, orientation and composition. *Polym. Test.* 40, 218–224. doi:10.1016/j.polymertesting.2014.09.009

Kędziora, A., Speruda, M., Krzyżewska, E., Rybka, J., Łukowiak, A., and Bugla-Płoskońska, G. (2018). Similarities and differences between silver ions and silver in nanoforms as antibacterial agents. *Int. J. Mol. Sci.* 19 (2), 444. doi:10.3390/ijms19020444

Khaydarov, R. A., Khaydarov, R. R., Gapurova, O., Estrin, Y., and Scheper, T. (2008). Electrochemical method for the synthesis of silver nanoparticles. *J. Nanoparticle Res.* 11 (5), 1193–1200. doi:10.1007/s11051-008-9513-x

Kim, J., Yeom, M., Lee, T., Kim, H.-O., Na, W., Kang, A., et al. (2020). Porous gold nanoparticles for attenuating infectivity of influenza A virus. *J. Nanobiotechnology* 18 (1), 54. doi:10.1186/s12951-020-00611-8

Kourmentza, C., Costa, J., Azevedo, Z., Servin, C., Grandfils, C., De Freitas, V., et al. (2018). Burkholderia thailandensis as a microbial cell factory for the bioconversion of used cooking oil to polyhydroxyalkanoates and rhamnolipids. *Bioresour. Technol.* 247, 829–837. doi:10.1016/j.biortech.2017.09.138

Lahiri, D., Nag, M., Sheikh, H. I., Sarkar, T., Edinur, H. A., Pati, S., et al. (2021). Microbiologically-synthesized nanoparticles and their role in silencing the biofilm signaling cascade. *Front. Microbiol.* 12, 636588. doi:10.3389/fmicb.2021.636588

Leifert, A., Pan-Bartnek, Y., Simon, U., and Jahnen-Dechent, W. (2013). Molecularly stabilised ultrasmall gold nanoparticles: synthesis, characterization and bioactivity. *Nanoscale* 5 (14), 6224. doi:10.1039/c3nr00916e

Lim, J., Yeap, S. P., Che, H. X., and Low, S. C. (2013). Characterization of magnetic nanoparticle by dynamic light scattering. *Nanoscale Res. Lett.* 8 (1), 381. doi:10.1186/1556-276X-8-381

Liu, D., Li, L., and You, T. (2017). Superior catalytic performances of platinum nanoparticles loaded nitrogen-doped graphene toward methanol oxidation and hydrogen evolution reaction. *J. Colloid Interface Sci.* 487, 330–335. doi:10.1016/j.jcis.2016.10.038

Locarno, S., Bucci, R., Impresari, E., Luisa Gelmi, Maria, Pellegrino, S., and Clerici, F. (2021). Ultrashort peptides and gold nanoparticles: influence of constrained amino acids on colloidal stability. *Front. Chem.* 9, 736519. doi:10.3389/fchem.2021.736519

Lukasiewicz, B., Basnett, P., Nigmatullin, R., Matharu, R., Knowles, J. C., and Roy, I. (2018). Binary polyhydroxyalkanoate systems for soft tissue engineering. *Acta Biomater.* 71 (71), 225–234. doi:10.1016/j.actbio.2018.02.027

Maddikeri, G. L., Pandit, A. B., and Gogate, P. R. (2012). Intensification approaches for biodiesel synthesis from waste cooking oil: A review. *Industrial Eng. Chem. Res.* 51 (45), 14610–14628. doi:10.1021/ie301675j

Madhusoodanan, G., Hariharapura, R. C., and Somashekara, D. (2021). Dissolved oxygen as a propulsive parameter for polyhydroxyalkanoate production using Bacillus endophyticus cultures. *Environ. Dev. Sustain.* 24 (4), 4641–4658. doi:10.1007/s10668-021-01626-3

Menzies, K. L., and Jones, L. (2010). The impact of contact angle on the biocompatibility of biomaterials. *Optometry Vis. Sci.* 87 (6). doi:10.1097/opx.0b013e3181da863e

Mohd Yusof, H., Mohamad, R., Zaidan, U. H., and Abdul Rahman, N. A. (2019). Microbial synthesis of zinc oxide nanoparticles and their potential application as an antimicrobial agent and a feed supplement in animal industry: A review. *J. Animal Sci. Biotechnol.* 10 (1), 57. doi:10.1186/s40104-019-0368-z

Moralejo-Gárate, H., Kleerebezem, Robbert, Anuska Mosquera-Corral and, C. M, M., and van Loosdrecht, M. C. (2013). Impact of oxygen limitation on glycerol-based biopolymer production by bacterial enrichments. *Water Res.* 47 (3), 1209–1217. doi:10.1016/j.watres.2012.11.039

Możejko, J., and Ciesielski, S. (2013). Saponified waste palm oil as an attractive renewable resource for mcl-polyhydroxyalkanoate synthesis. *J. Biosci. Bioeng.* 116 (4), 485–492. doi:10.1016/j.jbiosc.2013.04.014

Możejko-Ciesielska, J., and Kiewisz, R. (2016). Bacterial polyhydroxyalkanoates: still fabulous?. *Microbiol. Res.* 192, 271–282. doi:10.1016/j.micres.2016.07.010

Murray, C. J., Ikuta, K. S., Sharara, F., Swetschinski, L., Robles Aguilar, G., Gray, A., et al. (2022). Global burden of bacterial antimicrobial resistance in 2019: A systematic analysis. *Lancet* 399 (10325), 629–655. doi:10.1016/S0140-6736(21)02724-0

Naikoo, G. A., Mustaqeem, M., Hassan, I. U., Awan, T., Arshad, F., Salim, H., et al. (2021). Bioinspired and green synthesis of nanoparticles from plant extracts with antiviral and antimicrobial properties: A critical review. *J. Saudi Chem. Soc.* 25 (9), 101304. doi:10.1016/j.jscs.2021.101304

National Institutes of Health (2020). New coronavirus stable for hours on surfaces. Available at: https://www.nih.gov/news-events/news-releases/new-coronavirus-stable-hours-surfaces.

Nichols, R. J., Das, A. K., and Guha, A. K. (2009). Gold nanoparticles: microbial synthesis and application in water hygiene management. *Langmuir* 25 (14), 8192–8199. doi:10.1021/la900585p

Okkeh, M., Bloise, N., Restivo, E., De Vita, L., Pallavicini, P., and Visai, L. (2021). Gold nanoparticles: can they be the next magic bullet for multidrug-resistant bacteria?. *Nanomaterials* 11 (2), 312. doi:10.3390/nano11020312

Pallipurath, A., Nicoletti, O., Skelton, J. M., Mahajan, S., Midgley, P. A., and Elliott, S. R. (2014). Surfactant-free coating of thiols on gold nanoparticles using sonochemistry: a study of competing processes. *Ultrason. Sonochemistry* 21 (5), 1886–1892. doi:10.1016/j.ultsonch.2014.03.014

Palza, H. (2015). Antimicrobial polymers with metal nanoparticles. *Int. J. Mol. Sci.* 16 (1), 2099–2116. doi:10.3390/ijms16012099

Papp, I., Sieben, C., Ludwig, K., Roskamp, M., Böttcher, C., Schlecht, S., et al. (2010). Inhibition of influenza virus infection by multivalent sialic-acid-functionalized gold nanoparticles. *Small* 6 (24), 2900–2906. doi:10.1002/smll.201001349

Peschel, G., Dahse, H.-M., Konrad, A., Wieland, G. D., Mueller, P.-J., Martin, D. P., et al. (2008). Growth of keratinocytes on porous films of poly(3-hydroxybutyrate) and poly(4-hydroxybutyrate) blended with hyaluronic acid and chitosan. *J. Biomed. Mater. Res. Part A* 85A (4), 1072–1081. doi:10.1002/jbm.a.31666

Piktel, E., Suprewicz, Ł., Depciuch, J., Chmielewska, S., Skłodowski, K., Daniluk, T., et al. (2021). Varied-shaped gold nanoparticles with nanogram killing efficiency as potential antimicrobial surface coatings for the medical devices. *Sci. Rep.* 11 (1), 12546. doi:10.1038/s41598-021-91847-3

Quillaguamán, J., Guzmán, H., Van-Thuoc, D., and Hatti-Kaul, R. (2009). Synthesis and production of polyhydroxyalkanoates by halophiles: current potential and future prospects. *Appl. Microbiol. Biotechnol.* 85 (6), 1687–1696. doi:10.1007/s00253-009-2397-6

Rai, R., Yunos, D. M., Boccaccini, A. R., Knowles, J. C., Barker, I. A., Howdle, S. M., et al. (2011). Poly-3-hydroxyoctanoate P(3HO), a medium chain length polyhydroxyalkanoate homopolymer from Pseudomonas mendocina. *Biomacromolecules* 12 (6), 2126–2136. doi:10.1021/bm2001999

Rajendran, A. (2017). Antibacterial properties and mechanism of gold nanoparticles obtained from pergularia daemia leaf extract. *J. Nanomedicine Res.* 6 (1). doi:10.15406/jnmr.2017.06.00146

Rakowska, P. D., Tiddia, M., Faruqui, N., Bankier, C., Pei, Y., Pollard, A. J., et al. (2021). Antiviral surfaces and coatings and their mechanisms of action. *Commun. Mater.* 2 (1), 53–19. doi:10.1038/s43246-021-00153-y

Reidy, B., Haase, A., Luch, A., Dawson, K., and Lynch, I. (2013). Mechanisms of silver nanoparticle release, transformation and toxicity: A critical review of current knowledge and recommendations for future studies and applications. *Materials* 6 (6), 2295–2350. doi:10.3390/ma6062295

Riberio da Cuncha, B., Fonseca, L., and Calado, C. (2019). Antibiotic discovery: where have we come from, where do we go?. *Antibiotics* 8 (2), 45. doi:10.3390/antibiotics8020045

Ruiz, C., Kenny, S. T., Babu P, R., Walsh, M., Narancic, T., and O'Connor, K. E. (2019a). High cell density conversion of hydrolysed waste cooking oil fatty acids into medium chain length polyhydroxyalkanoate using Pseudomonas putida KT2440. *Catalysts* 9 (5), 468. doi:10.3390/catal9050468

Ruiz, C., Kenny, S. T., Narancic, T., Babu, R., and Connor, K. O. (2019b). Conversion of waste cooking oil into medium chain polyhydroxyalkanoates in a high cell density fermentation. *J. Biotechnol.* 306, 9–15. doi:10.1016/j.jbiotec.2019.08.020

Ladhari, Safa, Vu, N.-N., Boisvert, C., Saidi, A., and Nguyen-Tri, P. (2023). Recent development of polyhydroxyalkanoates (PHA)-Based materials for antibacterial applications: A review. *ACS Appl. Bio Mater.* 6. doi:10.1021/acsabm.3c00078

Sánchez-Clemente, R., Guijo, M. I., Nogales, J., and Blasco, R. (2020). Carbon source influence on extracellular pH changes along bacterial cell-growth. *Genes* 11 (11), 1292. doi:10.3390/genes11111292

Sengupta, P., and Prasad, V. (2018). Surface modification of polymers for tissue engineering applications: arginine acts as a sticky protein equivalent for viable cell accommodation. *ACS Omega* 3 (4), 4242–4251. doi:10.1021/acsomega.8b00215

Shamaila, S., Zafar, N., Riaz, S., Sharif, R., Nazir, J., and Naseem, S. (2016). Gold nanoparticles: an efficient antimicrobial agent against enteric bacterial human pathogen. *Nanomaterials* 6 (4), 71. doi:10.3390/nano6040071

Shameli, K., Ahmad, M. B., Jazayeri, S. D., Shabanzadeh, P., Sangpour, P., Jahangirian, H., et al. (2012). Investigation of antibacterial properties silver nanoparticles prepared via green method. *Chem. Central J.* 6 (1), 73. doi:10.1186/1752-153x-6-73

Sharon, M. (2012). Extracellular synthesis of gold nanoparticles using Pseudomonas denitrificans and comprehending its stability. Available at: https://www.academia.edu/17728829/Extracellular_Synthesis_of_Gold_Nanoparticles_Using_Pseudomonas_denitrificans_and_Comprehending_its_Stability.)

Silambarasan, S., and Abraham, J. (2012). Biosynthesis of silver nanoparticles using the bacteria Bacillus cereus and their antimicrobial property. *Int. J. Pharm. Pharm. Sci.*

Slavin, Y. N., Asnis, J., Häfeli, U. O., and Bach, H. (2017). Metal nanoparticles: understanding the mechanisms behind antibacterial activity. *J. Nanobiotechnology* 15 (1), 65. doi:10.1186/s12951-017-0308-z

Song, J. H., Jeon, C. O., Choi, M. H., Yoon, S. C., and Park, W. (2008). Polyhydroxyalkanoate (PHA) production using waste vegetable oil by Pseudomonas sp. strain DR2. *J. Microbiol. Biotechnol.* 18 (8), 1408–1415.

Souza, T. G. F., Ciminelli, V. S. T., and Mohallem, N. D. S. (2016). A comparison of TEM and DLS methods to characterize size distribution of ceramic nanoparticles. *J. Phys. Conf. Ser.* 733, 012039. doi:10.1088/1742-6596/733/1/012039

Su, C., Huang, K., Li, H.-H., Lu, Y.-G., and Zheng, D.-L. (2020). Antibacterial properties of functionalized gold nanoparticles and their application in oral biology. *J. Nanomater.* 2020. doi:10.1155/2020/5616379

Suresh, A. K., Pelletier, D. A., Wang, W., Broich, M. L., Moon, J.-W., Gu, B., et al. (2011). Biofabrication of discrete spherical gold nanoparticles using the metal-reducing bacterium Shewanella oneidensis. *Acta Biomater.* 7 (5), 2148–2152. doi:10.1016/j.actbio.2011.01.023

Suriyakala, G., Sathiyaraj, S., Babujanarthanam, R., Alarjani, K. M., Hussein, D. S., Rasheed, R. A., et al. (2022). Green synthesis of gold nanoparticles using Jatropha integerrima Jacq. flower extract and their antibacterial activity. *J. King Saud Univ. - Sci.* 34 (3), 101830. doi:10.1016/j.jksus.2022.101830

Suvarna, S., Das, U., Kc, S., Mishra, S., Sudarshan, M., Saha, K. D., et al. (2017). Synthesis of a novel glucose capped gold nanoparticle as a better theranostic candidate. *PLoS ONE* 12 (6), e0178202. doi:10.1371/journal.pone.0178202

Teimouri, M., Khosravi-Nejad, F., Attar, F., Saboury, A. A., Kostova, I., Benelli, G., et al. (2018). Gold nanoparticles fabrication by plant extracts: synthesis, characterization, degradation of 4-nitrophenol from industrial wastewater, and insecticidal activity – a review. *J. Clean. Prod.* 184, 740–753. doi:10.1016/j.jclepro.2018.02.268

van Doremalen, N., Bushmaker, T., Morris, D. H., Holbrook, M. G., Gamble, A., Williamson, B. N., et al. (2020). Aerosol and surface stability of SARS-CoV-2 as compared with SARS-CoV-1. *N. Engl. J. Med.* 382 (16), 1564–1567. doi:10.1056/nejmc2004973

Verlinden, R. A., Hill, D. J., Kenward, M. A., Williams, C. D., Piotrowska-Seget, Z., and Radecka, I. K. (2011). Production of polyhydroxyalkanoates from waste frying oil by Cupriavidus necator. *Amb. Express* 1 (1), 11. doi:10.1186/2191-0855-1-11

Vidal-Mas, J., Resina-Pelfort, O., Haba, E., Comas, J., Manresa, A., and Vives-Rego, J. (2001). Rapid flow cytometry – nile red assessment of PHA cellular content and heterogeneity in cultures of *Pseudomonas aeruginosa* 47T2 (NCIB 40044) grown in waste frying oil. *Antonie Leeuwenhoek* 80 (1), 57–63. doi:10.1023/a:1012208225286

World Health Organization (2022). Tracking SARS-CoV-2 variants. https://www.who.int/activities/tracking-SARS-CoV-2-variants.

World Health Organization (2023). Coronavirus disease (COVID-19). [online] Available at: https://www.who.int/news-room/fact-sheets/detail/coronavirus-disease-(covid-19)?fbclid=IwAR1jWK0VjID9aNb-A76mj2FXoz8C9tDn3bJxn9u5r1dewhnhUyQFoEvQA-8.

Xie, M., Xu, Y., Huang, J., Li, Y., Wang, L.-Y., Yang, L., et al. (2020). Going even smaller: engineering sub-5 nm nanoparticles for improved delivery, biocompatibility, and functionality. *Wiley Interdiscip. Reviews-nanomedicine Nanobiotechnology* 12 (6), e1644. doi:10.1002/wnan.1644

Yallappa, S., Manjanna, J., Peethambar, S. K., Rajeshwara, A. N., and Satyanarayan, N. D. (2013). Green synthesis of silver nanoparticles using Acacia farnesiana (sweet Acacia) seed extract under microwave irradiation and their biological assessment. *J. Clust. Sci.* 24 (4), 1081–1092. doi:10.1007/s10876-013-0599-7

Yugandhar, P., Vasavi, T., Jayavardhana Rao, Y., Uma Maheswari Devi, P., Narasimha, G., and Savithramma, N. (2018). Cost effective, green synthesis of copper oxide nanoparticles using fruit extract of syzygium alternifolium (wt) walp, characterization and evaluation of antiviral activity. *J. Clust. Sci.* 29 (4), 743–755. doi:10.1007/s10876-018-1395-1

Zhang, L., Li, R., Dong, F., Tian, A., Li, Z.-J., and Dai, Y. (2015). Physical, mechanical and antimicrobial properties of starch films incorporated with ε-poly-l-lysine. *Food Chem.* 166, 107–114. doi:10.1016/j.foodchem.2014.06.008